Volume 15, Issue 3, 152535 (1-11)

Iranian Journal of Catalysis (IJC)

https://doi.org/10.57647/j.ijc.2025.1503.35

Synthesis and characterization of a $CNT/Fe_2O_3/TiO_2$/Bentonite nanocomposite for photocatalytic degradation of tetracycline hydrochloride

Ayad Dari*, Mohammed Shorbaz, May Ali, Ahmed Zamil

Department of Chemical Engineering, University of Technology-Iraq Baghdad, Iraq.

***Corresponding author:** ayad.d.jaafar@uotechnology.edu.iq

Original Research

Received:
11 March 2025
Revised:
3 June 2025
Accepted:
10 July 2025
Published online:
21 July 2025
Published in issue:
30 September 2025

Abstract:

This process studies the efficiency of the advanced oxidation processes, which were used to decompose tetracycline hydrochloride in aqueous solutions by $CNT/Fe_2O_3/TiO_2$/Bentonit. A nanocatalyst was prepared with high conductivity, broad light absorption, and high surface area, utilizing Photocatalysts again. Several process variables (irradiation time, contaminant concentration, catalyst dosage, and pH) were studied. X-ray diffraction analysis. The quality of the high-performance nanocomposite catalyst construction will be improved if X-ray diffraction (XRD) shows that the catalyst has been transformed into a pure homogeneous structure. At pH 5, the contaminant was degraded in 120 min with a dose of 15 mg of the nanocomposite. At a concentration of 0.5 ppm tetracycline hydrochloride, the clearance rate reached 95.1%. The removal rate decreased with increasing pH, while titanium oxide degraded the tetracycline hydrochloride, bentonite, and nanocarbon exhibited contaminant adsorption capacity. The regression coefficient (R^2) of 0.97 indicated that the process best conformed to quasi-first-order kinetics.

Keywords: Advanced oxidation; Removal; Renewable; Reactor; Treatment

1. Introduction

Antibiotics have been widely used in recent years to treat human diseases, and they are also added to animal feed to encourage growth and maintain animal health Given their high biological activity, especially in soil and water, and the negative environmental effects of these toxic and long-lasting antibiotics, there is a potential for excessive environmental pollution resulting from their misuse [1]. The body excretes 90% of the original dose of antibiotics ingested by humans. Because most tetracyclines are poorly absorbed by humans and animals, these high levels of excretion harm the environment. It is widely used in animal feed in China, the United States, India, and other countries [2]. Commonly used antibiotics are classified into tetracyclines (TCs), macrolides, and other groups based on their chemical structure. Researchers and environmentalists are concerned about the presence of antibiotics in water and their potential transfer to drinking water [3]. As a result, when these substances reach non-target organisms, they cause undesirable changes, including genotoxicity and gene expression that is harmful to humans [4].

Doctors have returned to using tetracycline hydrochloride and other tetracycline antibiotics for many reasons, including [5, 6]. Resistance to modern antibiotics such as cephalosporins and fluoroquinolones has made it necessary to resort to old antibiotics such as tetracycline, which is still effective against some resistant strains [7, 8]. In addition, tetracycline has proven effective against some resistant strains such as Acinetobacter and some types of Rickettsia [9, 10]. It is used to treat acne, sexually transmitted diseases such as chlamydia, typhoid, borreliosis (Lyme disease), and some types of respiratory tract infections. Some tetracyclines have anti-inflammatory properties, making them an option in non-bacterial conditions, such as granulomatosis and arthritis [11]. TC is a well-known antibacterial agent that is widely used in treating [12]. Finally, it is sometimes

used as a preventive measure in some epidemics caused by bacteria, especially in areas with limited medical resources [13]. The return of tetracycline use is not evidence of its superiority over modern antibiotics, but rather an inevitable result of the emergence of bacterial resistance and the ongoing search for effective alternatives to treat antibiotic-resistant infections [14, 15].

According to studies, small amounts of tetracycline are found in the environment, especially in treated wastewater, and high levels in hospital and pharmaceutical wastewater ($100-500$ mg/L) [3, 16]. The broad-spectrum antibiotic, tetracycline, is commonly found in drinking water (11 ng/L), groundwater (0.4 μg/kg) [3], sediments (126 μg/kg), mariculture (259.1 ng/L), and landfills (63.8 μg/kg) [17]. The total concentration of tetracycline in inlet water was 0.001616 ppm, while in wastewater it was 195 ng/L [18].

Initial treatments only partially removed these contaminants, and tens of nanograms/liter of these antibiotics remained in the wastewater. Advanced oxidation technologies were used to detoxify the antibiotic-contaminated water [19].

Many researchers have conducted studies on tetracycline removal, and photocatalytic degradation is one of several treatment methods [20]. To break down and remove contaminants in the liquid, advanced biological coagulation processes, ultrasound procedures, adsorption, and photocoagulation have been investigated [17].

Extensive research has been conducted on titanium dioxide-based photocatalysis for advanced oxidation due to its low cost, stability, and high deposit removal efficiency. However, catalyst aggregation and difficulty in recovering it at the nanoscale are drawbacks that hinder the photocatalysis process, which has led some researchers to develop composite nanomaterials [21].

The easily synthesized bentonite complex with nano-titanium oxide enhances the surface area of the catalyst, which in turn increases the process efficiency [22, 23]. Carbon nanotubes were added as non-metals and metals to develop TiO_2 and overcome its disadvantages [24]. Numerous studies have demonstrated the efficient production of titanium oxide using carbon nanotubes. The preparation of metal-supported catalysts relies on multi-walled carbon nanotubes, which offer broad light absorption, a large surface area, and high conductivity [25].

By capturing and holding titanium dioxide electrons, multi-walled carbon nanotubes can perform electron recombination, resulting in electron pair separation [26]. To reduce titanium dioxide aggregation, the carbon nanotubes act as a scattering layer. Recently, I used nanotubes to produce self-packed Fe_3O_4 nanoparticles [24].

Nano carbon, iron oxide, titanium oxide, and bentonite are used in the removal of tetracycline from water by advanced oxidation processes (AOPs) for the most important reasons of adsorption efficiency and improved photocatalytic activity [27, 28]. A bentonite with a high surface area helps in the adsorption of tetracycline from water, making it easier to break down later [29, 30]. Graphene enhances adsorption due to its large surface area and interaction with organic pollutants [31]. In addition, titanium oxide (TiO_2) is a strong and cheap photocatalyst that absorbs ultraviolet light, generating hydroxyl radicals ($^{\bullet}OH$) that break down tetracycline into less harmful compounds [32, 33]. It is characterized by chemical stability and reusability [34].

Addition of iron oxide (Fe_3O_4): It acts as a co-catalyst to catalyze the Fenton reaction when hydrogen peroxide (H_2O_2) is added, which produces strong free radicals to break down tetracycline. It imparts a magnetic property to the material, making it easy to recover after treatment, and thus it can be reused [35, 36]. The combination of adsorption (bentonite + nanocarbon), photocatalysis (TiO_2), and Fenton reaction catalysis (Fe_3O_4) leads to efficient and rapid degradation of tetracycline without leaving toxic by-products [37, 38]. This combination increases the reaction rate and reduces the energy requirement compared to using TiO_2 alone [39, 40]. This nanocatalyst enables high surface area, enhanced electron transfer, and synergistic adsorption and decomposition mechanisms at interfaces, providing new insights into the design of efficient and reusable nanocatalysts for advanced oxidation processes [41].

In this context, this study pioneers the synthesis and characterization of a novel multicomponent nanocomposite composed of carbon nanotubes (CNTs), iron oxide (Fe_3O_4), titanium dioxide (TiO_2), and bentonite clay. By integrating CNTs, known for their exceptional electrical conductivity and surface area, with Fe_3O_4 and TiO_2 nanoparticles anchored to the layered structure of bentonite, the composite exhibits a unique structure designed to enhance charge separation, extend light absorption into the visible region, and provide abundant active sites for photocatalytic reactions [42]. This strategic combination not only mitigates the drawbacks of pure TiO_2 but also introduces synergistic interactions between the components, leading to a significant improvement in the photocatalytic degradation efficiency of tetracycline hydrochloride. One of the most significant advances in this work lies in the specially designed interface engineering between the semiconductor phases (TiO_2 and Fe_3O_4) and the conductive carbon nanotube network supported by the bentonite matrix [43]. The hierarchical structure promotes efficient charge transport pathways and reduces recombination losses, amplifying the photocatalytic activity under visible light irradiation. Furthermore, the incorporation of natural bentonite provides mechanical stability, reusability, and environmental friendliness to the nanocomposite, enabling a scalable pathway for environmental applications [44].

The synergy between TiO_2 and Fe_3O_4 enables efficient light harvesting and enhanced redox potential. Because TiO_2 is a wide-bandgap semiconductor (~ 3.2 eV), it is primarily activated under ultraviolet light; however, the presence of Fe_3O_4 (~ 2.2 eV) extends the light absorption range into the visible region. Fe_3O_4 also acts as an electron mediator, facilitating electron transfer from TiO_2 and delaying charge recombination [42].

The carbon nanotubes (CNTs) in this composite perform a dual role. First, they act as electron acceptors and conductive pathways, improving electron mobility. Second, their high surface area supports the adsorption of carbon nanoparticles, increasing their availability at reactive sites [45]. Bentonite, as a layered clay material, helps disperse

the nanoparticles and provides additional adsorption sites, facilitating the reaction of the contaminant with the catalyst. Ultimately, the efficient generation of hydroxyl radicals and superoxide via photoinduced electron–hole pairs, combined with improved charge separation by Fe_3O_4 and CNTs, promotes the degradation of the carbon nanotubes. The degradation mechanism involves lower initial adsorption, radical attack, fragmentation of the carbon nanostructure, and eventual mineralization into non-toxic end products [46].

From a surface and interface science perspective, this study provides new insights into the design and optimization of multiphase heterojunctions [47]. It also significantly deepens the understanding of how electron transfer is facilitated across complex hybrid interfaces and how surface properties, such as porosity, adsorption affinity, and catalytic site distribution, affect performance. Furthermore, the research highlights the importance of synergistic coupling effects and defect engineering in tailoring photocatalyst properties at the nanoscale. Thus, these results contribute to advancing this field by demonstrating how intelligently designed multicomponent composites can embody fundamental surface science with practical environmental solutions, setting a new standard for high-performance and sustainable photocatalytic systems [48].

Xinni Sun, The lack of an efficient photocatalyst that can be well integrated with the membrane limits the development of photocatalytic membrane reactor (PMR), which is gaining more and more interest in the purification of water bodies contaminated with antibiotics [49].

L. Sun, use materials with dual absorption and photocatalytic capabilities. This study describes the efficient fabrication of a novel S-system heterogeneous photocatalyst, InVO4/ZnIn2S4, featuring a unique hierarchical structure that provides multiple readily accessible absorption/photocatalytic sites. After 15 minutes, the synergistic tetracycline removal rate reached 69.31%, and after 45 minutes, 69.31% [50].

The poor contact between silver/titanium dioxide composites was a major obstacle to increasing the photodegradation activity of tetracycline (TC). Therefore, Xia used nitrogen (Ni) intercalation and nitrogen (Ns) substitution techniques in this study to produce silver/titanium dioxide composites. The results showed that after 60 minutes of visible light exposure, the degradation efficiency of the silver/titanium dioxide composite increased to 90% [51].

Using a nano-titanium dioxide-coated carbon membrane through sol-gel technology, an electrocatalytic membrane was constructed to degrade aqueous tetracycline (TC). With an initial concentration of 50 ppm tetracycline (pH $3.8-9.6$), it could be efficiently removed by the electrocatalytic membrane. At a temperature of 25 °C and a residence time of 4.4 min, the following operating parameters could lead to 100% tetracycline removal [52].

The study aimed to develop a specially modified catalyst that enhances the degradation of tetracycline under all conditions while being easy to recover and reuse. The effects of pH, reaction mechanism, catalyst quantity, tetracycline concentration, and time were studied.

2. Experimental section

2.1 Catalyst preparation

To ensure complete dispersion of the contaminants in the solution, the solution was mixed for 120 minutes with the required amount of synthesized catalyst nanoparticles and magnetically spun in the dark. The UV light, located at the center of the reactor, was then turned on. An external water-cooling system was used around the reactor to maintain the temperature during the process experiments.

Forty milliliters of ethanol were mixed with one gram of carbon nanotubes for two hours, and then five grams of $Fe(NO_3)_3{\cdot}9H_2O$ were added for an additional two hours. A beaker containing 400 mg of carbon nanotubes/Fe_2O_3 was placed in an ultrasonic bath for 15 minutes after stirring and cleaning. A mixture of slightly dilute hydrochloric acid and 40 milliliters of ethanol was then added. The mixture was then mixed with a titanium dioxide/bentonite mixture and shaken to form a gel structure. The mixture was cooled for two hours. Subsequently, the mixture was dried in an oven at 70 °C. After washing with water several times, the mixture was cooled and separated by centrifugation. After granulation, the samples were dried in an oven [22].

Under irradiation with photons of energy equal to or greater than the band gaps of TiO_2 (~ 3.2 eV) and Fe_2O_3 (~ 2.2 eV), both semiconductors become photoactive:

$$TiO_2 + h\nu \rightarrow e^-_{CB,TiO_2} + h^+_{VB,TiO_2} \quad (1)$$

$$Fe_2O_3 + h\nu \rightarrow e^-_{CB,Fe_2O_3} + h^+_{VB,Fe_2O_3} \quad (2)$$

[53]

Electrons move from the basal surface of Fe_2O_3 to the basal surface of TiO_2. Holes move from the basal surface of TiO_2 to the basal surface of Fe_2O_3. This charge transfer reduces recombination and maintains high redox potentials at the respective bands.

The photogenerated electrons are efficiently captured and transported by the carbon nanotubes. The carbon nanotubes delay the recombination of electrons and holes and transfer the electrons to the oxygen adsorbed on the surface.

$$CNT + e^- \rightarrow CNT(e^-) \quad (3)$$

Dissociated charge carriers initiate redox reactions on the surface: reduction of oxygen by electrons (either from titanium dioxide or via carbon nanotubes).

$$e^- + O_2 \rightarrow^{\bullet} O_2^- \quad (4)$$

[54]

Oxidation of water or hydroxide by holes:

$$h^+ + H_2O \rightarrow^{\bullet} OH + H^+ \quad (5)$$

$$h^+ + OH^- \rightarrow^{\bullet} OH \quad (6)$$

$$^{\bullet}OH/^{\bullet}O_2^- + TC \rightarrow \text{intermediates} \rightarrow CO_2 + H_2O + NO_3^- + NH_4^+ \quad (7)$$

[55, 56]

To determine the mechanism behind tetracycline hydrochloride removal, the resulting nanoparticles were analyzed using BET, SEM, TEM, XRD, FT-IR, and Raman analysis.

2.2 Chemicals

We purchased tetracycline hydrochloride TC ($C_{22}H_{24}O_8N_2$·HCl) with a purity greater than 95% from Sigma-Aldrich (Germany), (Merck 99.7%), titanium dioxide, $Fe(NO_3)_3$·$9H_2O$ (Sigma-Aldrich 98%), and bentonite (Sigma-Aldrich). For each step of the process, solutions were prepared with distilled water. All experiments were conducted in a laboratory-scale batch system at a constant temperature of 20 °C, using a Pyrex glass tube with an outer radius of 70 mm, an inner radius of 5 mm, and a length of 400 mm. The cylindrical photoreactor contained a low-pressure mercury UV lamp (TL 8 W BLB, Philips, Poland) with an output power of 8 W and a wavelength of 365 °F. Above it was a heating element (Model: HTS-1003, China).

2.3 Batch experiments

Batch experiments using CNT/Fe_2O_3/TiO_2/Bentonit nanocomposite. The solution was mixed using a magnetic stirrer, and the batch procedure was checked in a beaker. Photocatalytic tests were performed in a 500 mL AOP beaker. In the middle of the reactor was a UV. Nanocomposite CNT/Fe_2O_3/TiO_2/Bentonit, ranging from 0.5 mg/L to 15 mg/L, was used at room temperature. The irradiation time ranged from 120 min, and the pH ranged from 3 to 11. After adjusting the pH and adding catalytic nanoparticles, 100 mL of the contaminated solution was placed in the beaker. The pH of the solution was adjusted using a (WTW InoLab Cond 720) pH meter. To ensure uniform mixing of the mixture, the magnetic stirrer and UV lamp were operated at 250 rpm at the beginning of the experiment. After the experiment was completed, the material was carefully collected and evaluated using a UV spectrometer at 357 nm.

3. Results and discussion

3.1 Characterization studies

Using a scanning electron microscope (Hitachi, Japan model S-4160), microscopic images of the sample after dispersion of carbon nanotubes are shown in Fig. 1 (a), and it is clear that the particles are evenly distributed. With an average particle size of $25-55$ nm, the transmission electron microscope (TEM) showed that these nanoparticles are evenly distributed and visible within the carbon nanotube framework in Fig. 1 (b). Like carbon nanotubes, the CNT/Fe_2O_3/TiO_2/Bentonite composite photocatalyst is tubular. Due to the bentonite effect, pure carbon nanotubes tend to bend and aggregate with TiO_2, but the image shows that after mixing, there is a tubular distribution and no aggregation. The BET surface area of the nanocatalyst was determined to be 121 m^2/g.

Fig. 2 (a) shows the Fourier transform infrared (FT-IR) spectra of the as-prepared carbon nanotube (CNT)/iron oxide (Fe_2O_3)/titanium dioxide (TiO_2)/bentonite catalyst (Perkin-Elmer, USA). TiO_2 can be associated with the band at 600 cm^{-1}. This band corresponds to iron oxide (Fe_2O_3) at 1200 cm^{-1} and bentonite at 1000 cm^{-1}. Due to the oxidation of some carbon atoms on the nanocarbon surface, the carboxyl groups exhibit a hydroxyl band peak at 3800 cm^{-1}, while the free hydroxyl groups are located at 2900 cm^{-1}. This catalyst has FT-IR spectra that are very similar to those of nanocomposites previously published in scientific literature [57].

Raman Spectroscopy (type SENTERRA, Germany). The Raman spectrum exhibits several distinct peaks. This peak represents the vibration modes of the bentonite clay matrix at 500 cm^{-1}, typically associated with Si-O and Al-O bending vibrations. The peak at 700 cm^{-1} is attributed to Ti-O-Ti stretching modes in the anatase phase (TiO_2), indicating the presence of titanium dioxide nanoparticles. The peaks associated with Fe-O_3 vibrations within the Fe_2O_3 structure are found at 1000 cm^{-1}, confirming the presence of iron oxide. The peak at 1350 cm^{-1} (D band) represents the disorder-induced vibration mode in the carbon structure, which is common in multi-walled carbon nanotubes (MWCNTs). The peak at 1580 cm^{-1} (G band) is associated with the E_2g phonon of sp^2-bonded carbon atoms in graphitic materials, indicating the high crystallinity of the carbon nanotubes. The high density of the D and G bands confirms the successful integration of the carbon nanotubes

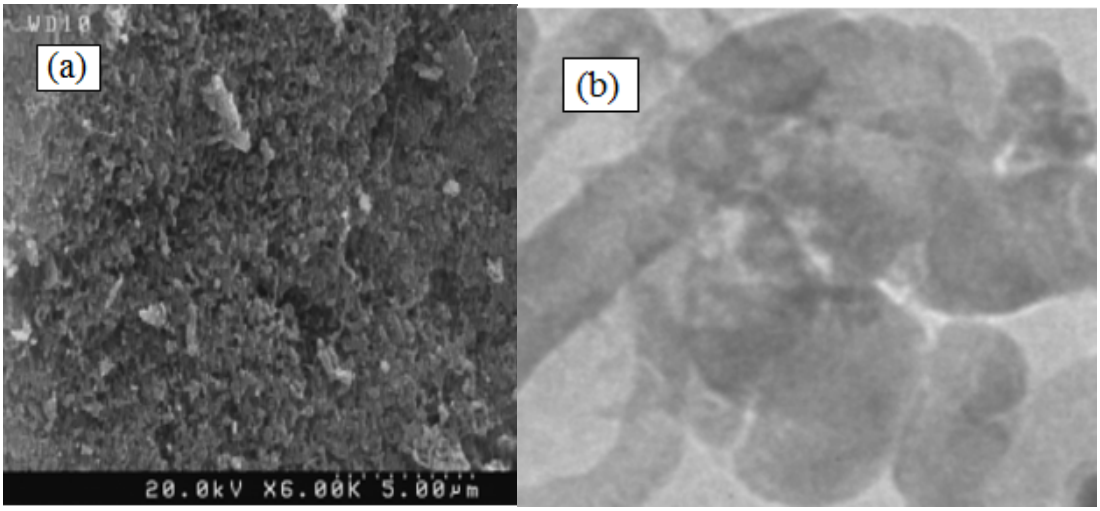

Figure 1. (a) SEM; (b) TEM image of CNT/Fe_2O_3/TiO_2/Bentonite nanocomposite catalyst.

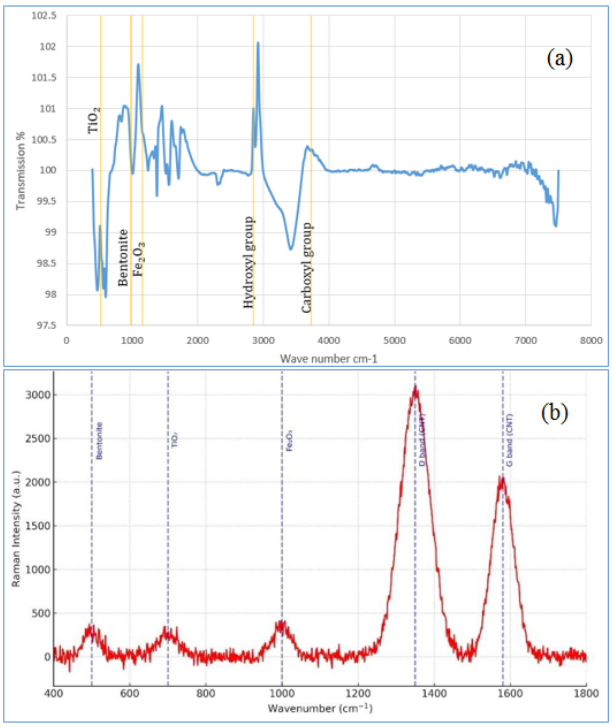

Figure 2. (a) FT-IR spectra of CNT/Fe_2O_3/TiO_2/Bentonite; (b) Raman spectrum of the CNT/Fe_2O_3/TiO_2/Bentonite nanocomposite.

within the composite, providing a conductive network that enhances electron transfer during photocatalytic reactions or AOP reactions, Fig. 2 (b).

Carbon nanotubes act as conductors and electron adsorbents for organic molecules due to their high surface area [58]. Meanwhile, the TiO_2 nanoparticles act as photoactive centers that generate reactive oxygen species when exposed to UV/visible light [59]. The Fe_2O_3 particles participate in Fenton-like reactions, producing hydroxyl radicals ($^{\bullet}OH$) under light, promoting the oxidative degradation of organic materials [60]. Bentonite clay provides mechanical stability, a high surface area, and a dispersion matrix that prevents nanoparticle aggregation, which is a key reason for its addition as a catalyst [61].

As a result, these synergistic effects significantly improve the material's photocatalytic and oxidative performance against the degradation of tetracycline. Raman analysis clearly demonstrates the successful fabrication of a composite material composed of carbon nanotubes, titanium dioxide, iron oxide, and bentonite. The presence of distinct peaks confirms the integrity of the material's structure and its potential for environmental remediation applications. X-ray diffraction (XRD) data show the absence of impurity phases (such as $FeTiO_3$ and Fe_3C), confirming phase stability. Peak intensity ratios indicate $Fe_2O_3 > TiO_2 >$ carbon nanotube concentration. The distribution is homogeneous, as evidenced by regular peak broadening and the absence of discrete phase peaks.

The hybrid structure promotes the generation of reactive species and facilitates efficient electron transfer, making it an excellent candidate for advanced oxidation processes (AOPs) aimed at degrading antibiotics such as tetracycline in water treatment applications. This approach offers a promising, sustainable, and effective strategy for mitigating pharmaceutical contamination [62].

The diffraction pattern for the nanocomposite is shown in Fig. 3 by model (PAN alytical X'Pert pro MPD, Netherlands). A sharp (002) peak for carbon nanotubes at 26.5° and a weaker (100) dip at 43° confirm the preservation of the graphitic system. In hematite (Fe_2O_3), the intense peaks at 35.5° (311), 51° (400), and 53° (422) correspond to the rhombic phase, indicating a well-crystalline oxide. In TiO_2, the reflections at 25.3° (101), 38.6° (004), 48.0° (200), and 75.0° (215) are unambiguously attributed to tetragonal anatase, without any detectable rutile or brookite inclusions. In bentonite (montmorillonite), the basal (001) is present at $\approx 15°$ but is markedly attenuated, indicating partial detachment or overlap. No outlier peaks (such as $FeTiO_3$ and Fe_3C) were observed, confirming the phase purity and successful complex formation without byproducts. This structural evolution enhances the dispersion of oxide nanocrystals and prevents clay re-stacking, thus maximizing the active surface area [63, 64].

The Debye-Scherrer equation (8) was also used to calculate the average sample crystal diameters (D) from the primary diffraction peaks.

$$D = \frac{0.94\lambda}{\beta \cos\theta} \tag{8}$$

where θ is the Bragg angle of the principal planes, β is the full width at half maximum (FWHM) of the diffraction peak in radians, and λ is the wavelength of the Cu Kα radiation. Williamson and Hall state that strain depends on the value of tan θ from the peak width and that crystal volume varies with a ratio of $1/\cos\theta$. Therefore, the following equation can be used to distinguish between the volume and strain contributions:

$$\beta_{hkl} \cos\theta = \frac{k\lambda}{D} + 4\varepsilon \sin\theta \tag{9}$$

where β_{hkl} is peak full width maximum corrected, ε is lattice strain.

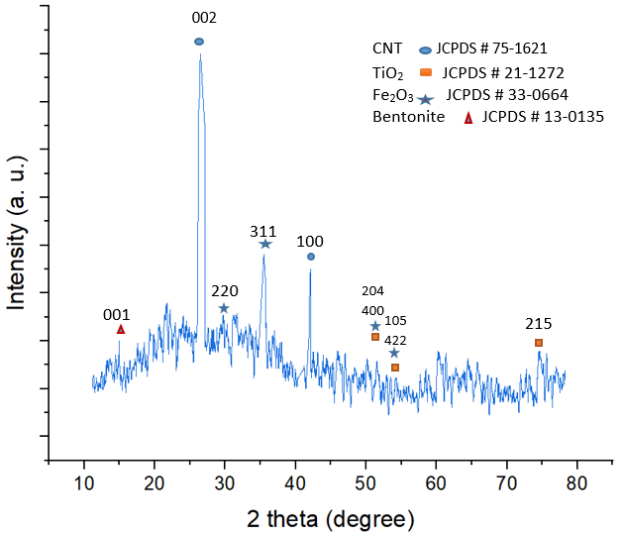

Figure 3. XRD pattern of CNT/Fe_2O_3/TiO_2/Bentonite nanocomposite.

According to the Debye-Scherrer equation, the typical crystal size is about $23-32$ nm, and the Williamson–Hall method is 34.4 nm, and the microstrain ε find is 7.1×10^{-4} [65].

BET analysis of the surface area showed a relatively high value of 121 m^2/g. This high surface area is consistent with the small crystal and particle sizes observed using X-ray diffraction (XRD) and transmission electron microscopy (TEM) and calculated from the Scherrer and Williamson-Hall model, and indicates a porous structure with a large external surface area available for adsorption or catalytic reactions with crystals a regular lattice structure. This surface area improves the photocatalytic and adsorption properties and plays an effective role in the removal of tetracycline.

3.2 Degradation process

In a 500-mL flask at 20 °C, batch samples were shaken with a shaker set at 250 rpm. Their effects on the decomposition reactions were studied using the following parameters: pH (3, 5, 7, 9, and 11), catalyst dosage (0.5, 5, 10, and 15 mg/L), and tetracycline concentration range (0.5, 5, 10, and 30 mg/L). The UV source was placed inside the reactor, and a tube surrounding the flask filled with cold water was used to cool the solution.

$$\text{Degradation Efficiency} = \frac{C_0 - C}{C_0} \times 100\% \qquad (10)$$

where: C_0, C = The concentrations of TC before and after degradation process.

3.2.1 Time of degradation

Under a variety of conditions, the effect of the time taken by UV radiation to degrade organic pollutants in a TC stock solution (120 min) was examined. The relationship between irradiation duration and TC removal by photocatalysis was examined using batch experiments. With 120 min being the maximum irradiation exposure duration and 80 min being the optimal irradiation exposure duration, Fig. 4 (a) shows that the percentage of TC removed increased by 95.1% with increasing irradiation time. Since photoremediation typically uses very little electricity (about 50% of the total operating cost), organic molecules are not degraded and maintain their chemical structures if the pretreatment period is short [22].

This improvement in degradation efficiency with longer irradiation time can be attributed to the increased generation of reactive oxygen species (ROS), such as hydroxyl radicals ($^{\bullet}OH$) and superoxygen anions ($O_2^{\bullet-}$), which actively participate in the degradation of complex organic molecules. During the initial stages of irradiation, the availability of active sites and photogenerated charge carriers is high, facilitating efficient interaction with TC molecules. As the reaction progresses, the TC concentration decreases, and the degradation rate gradually stabilizes due to the reduced availability of target molecules and the potential for electron-hole recombination [66].

It is worth noting that despite the low energy consumption associated with UV photocuring which accounts for approximately 50% of the total operational cost the efficiency of the process is significantly affected by the irradiation duration. Insufficient irradiation time can lead to incomplete degradation, as organic molecules retain their structural integrity without sufficient exposure to oxidizing species [67]. Therefore, optimizing radiation time is essential to achieve a balance between energy efficiency and effective pollutant removal, especially in large-scale wastewater treatment applications.

3.2.2 Effect of concentration

The effect of the initial tetracycline (TC) concentration on photodegradation efficiency was systematically evaluated under constant conditions: A reaction time of 120 min, pH 5, and a composite nanodosage of 15 mg/L, as shown in Fig. 4 (b). The results showed that the degradation efficiency peaked at 95.1% at the lowest tetracycline concentration (0.5 mg/L). However, as the concentration increased to 5, 10, and 30 mg/L, the efficiency gradually decreased to 91.8%, 83.3%, and 52%, respectively. This trend is commonly observed in photocatalytic systems and can be attributed to two main factors. Firstly, competition between tetracycline molecules for limited active sites on the photocatalyst surface, and secondly increased light absorption and scattering by the more concentrated tetracycline solution, leading to a decrease in the availability of photons for photoactivation [68].

Furthermore, while the degradation kinetics were evaluated over a standardized timeframe of 80 minutes, it was observed that at the highest concentration (30 mg/L), the degradation rate plateaued after 100 minutes. This plateau indicates the accumulation of intermediate degradation products, which may have adsorbed to the catalyst surface, deactivating the active sites and further inhibiting light absorption. Furthermore, the absorption of UV by TC molecules at higher concentrations significantly contributes to the reduced photocatalytic efficiency, as supported by previous studies and illustrated in figure 4 (b). Overall, these results emphasize the critical role of contaminant concentration in determining the efficiency of photocatalytic processes. Maintaining low contaminant levels is essential to maximize ROS production and ensure optimal photocatalytic activity [69].

3.2.3 Effect of CNT/Fe_2O_3/TiO_2/Bentonite Dosage

The amount of active sites within the element and the concentration of organic pollutants in the solution should interact to determine the photocatalytic dosage; thus, the more active sites, the better the catalyst performance. The effects of various CNT/Fe_2O_3/TiO_2/Bentonite dosages on the photodegradation of TC stock solution ($0.5-30$ mg/L) were investigated (pH = 5, conc. of TC = 0.5 mg/L). The efficiency results are shown in Fig. 4 (c). To increase the TC removal efficiency, composite dosages ranging from 0.5 to 5 mg/L were used; the TC removal was 35% and 50% when the irradiation duration was 120 min. The TC removal efficiency increased to 77% and 95.1% when the dosage was raised to 10 mg/L and 15 mg/L, respectively.

The photocatalytic performance of composite materials is significantly influenced by the availability of active surface sites, which facilitate the generation of reactive oxygen species required for the degradation of organic pollutants

[70]. Therefore, optimizing the photocatalyst dosage is essential to ensure efficient interaction between the catalyst and the target pollutants, such as tetracycline (TC), especially at varying concentrations. These results indicate that increasing the catalyst dosage provides more adsorption sites and active centers, promoting higher rates of hydroxyl radical and superoxide generation. However, excessive dosages, beyond a certain threshold, may lead to light scattering and reduced light transmission, potentially reducing photocatalytic efficiency, a phenomenon that warrants further research.

3.2.4 Effect oF pH

The pH level of the solution may be a key component of the photoactivity because it affects the surface charge of the photocatalyst and the production of hydroxyl radicals between hydroxyl ions and positive holes on the surface of the nanocomposite. At about pH 5, the resulting nanocomposite had a zero-point charge; this significantly affects the subsequent removal of TC, Fig. 4 (d). The optimum hydrolysis value was at pH 5 due to the continuous increase in the generated hydroxyl radicals [71].

In order to achieve the highest TC removal efficiency, the effect of pH at different values on the TC removal efficiency in photocatalytic processes using a nanocomposite (dosage = 15 mg/L; irradiation time = 120 min, and conc of TC = 0.5 mg/L) with variable pH was investigated. The highest TC removal efficiencies were 95.1% when the pH was at 5, and gradually decreased to the lowest removal efficiencies of (93.1, 94.2, 60 and 22.2%) when the pH was at 3, 7, 9, and 11. This is illustrated in Fig. 4 (d). As a result, decreasing the pH increases the active area of the catalyst. For a wide range of pH values, the surface charge of the catalyst may be affected, and the removal efficiency may be affected by the adsorbent molecules contacting the adsorbent surface.

Titanium oxide (TiO_2) acts as a photocatalyst when exposed to ultraviolet (UV) light. Electrons (e^-) and positive holes (h^+) are generated when light energy is absorbed by TiO_2. Redox reactions occur when positive holes (h^+) on the surface of TiO_2 oxidize water (H_2O) or hydroxyl (OH^-) molecules to form hydroxyl radicals ($^\bullet OH$), which are strong oxidizing agents capable of breaking down organic compounds such as tetracycline. The electrons (e^-) may reduce molecular oxygen (O_2) present in the solution to form superoxide radicals ($^\bullet O_2^-$) [72].

The role of iron oxide (Fe_2O_3) It helps to promote the production of oxidative radicals ($^\bullet OH$) and acts as an additional catalyst to facilitate electron transfer and improve the efficiency of breaking down [73]. Bentonite acts as a catalyst support and improves the surface distribution of the catalyst [74], while nanocarbon enhances the initial adsorption of tetracycline molecules from the solution onto its surface, increasing the reaction efficiency and reducing the recombination of electrons and positive holes. Crack Reaction Oxidative radicals ($^\bullet OH$ and $^\bullet O_2^-$) attack the chemical bonds of tetracycline molecules (such as C=C and C-N bonds). Tetracycline is broken down into intermediates such as short-chain organic acids, which are subsequently oxidized to carbon dioxide (CO_2) and water (H_2O) [75, 76].

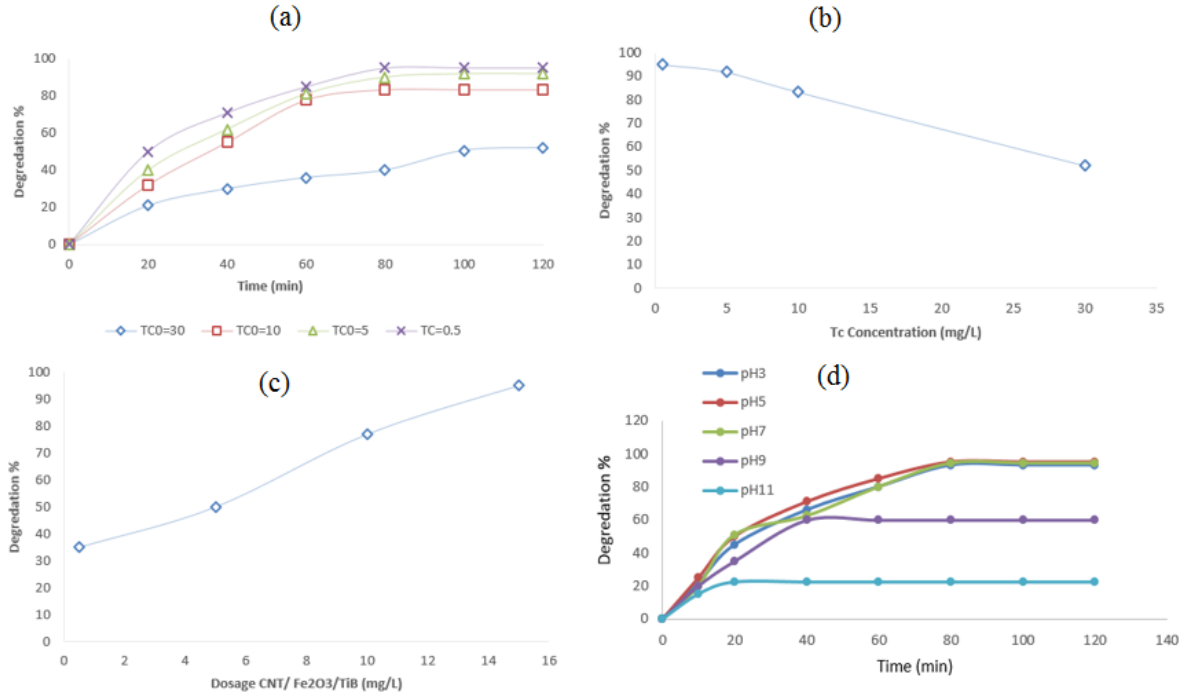

Figure 4. (a) At pH 5, the nanocomposite dosage is 15 mg/L, and the photolysis rate is affected by tetracycline hydrochloride concentrations (0.5, 5, 10 and 30 mg/L) over time (min). (b) At pH 5, 15 mg/L nanocomposite dosage is used to influence the TC concentrations (0.5, 5, 10 and 15 mg/L) for photolysis. (c) The effect of nanocomposite dosage on the degradation rate at pH 5, 0.5 mg/L tetracycline hydrochloride concentration, and degradation time (120 min). (d) The effect of pH on the photolysis rate over time (min), 15 mg/L nanocomposite dosage, and 0.5 mg/L tetracycline hydrochloride concentration.

3.3 Kinetic study

The photolysis of TC was studied kinetically using quasi-first-order and quasi-second-order models. Equation (11) represents the kinetic model (quasi-first-order) in its linear form.

$$\ln(\frac{C_0}{C}) = k1 \times t \quad (11)$$

where C_0 is the initial TC concentration (mg/L), C_0 is the observed rate constant (1/min), and C_0 is the TC concentration at time t (mg/L) and time (min).

Plotting $\ln(C_0/C)$ over time produces a straight line with slope $k1$. Equation (12) also represents the linear version of the kinetic (quasi-second-order) model.

$$\frac{1}{C} - \frac{1}{C_0} = k2 \times t \quad (12)$$

By plotting $(1/C) - (1/C_0)$ against time, a straight line with a slope of $k2$ is obtained.

The regression coefficient (R^2) of 0.97 for TC concentrations of 0.5 mg/L, Fig. 5 (a) perfectly matches the photodegradation of TC using the CNT/Fe_2O_3/TiO_2/Bentonite catalyst with quasi-first-order kinetics under all conditions, according to the results reported in (solution pH = 5, dosage = 15 mg/L, TC = 0.5 mg/L, irradiation time = 120 min). This result is consistent with the Kapp coefficient for photodegradation determined in one study. However, the regression coefficient (R^2) for the same condition, of 0.8, showed that quasi-second-order kinetics was less favorable in all cases, Fig. 5 (b) [54].

The kinetic data fit well with the pseudo-first-order model, yielding a high regression coefficient ($R^2 = 0.9716$), indicating that the degradation rate is directly proportional to the concentration of the TC molecule. This high degree of correlation suggests that the reaction likely follows a surface adsorption-degradation controlled process, where the availability of active sites on the photocatalyst plays a key role in determining the reaction rate. In contrast, the pseudo-second-order model was evaluated under similar conditions. Despite holding the pH, irradiation time, and initial TC concentration constant, the model yielded a lower regression coefficient ($R^2 = 0.8041$), indicating a poor fit. This suggests that the reaction mechanism under this dosage condition, i.e., the photocatalyst concentration, limits the availability of reactive sites required for such reactions.

The significant difference in regression coefficients between the two models ($\Delta R^2 = 0.1675$) confirms the importance of catalyst dosage in influencing the degradation kinetics. At higher dosages, the photocatalyst provides a greater active surface area, enhancing the likelihood of TC adsorption and subsequent photoreaction, favoring the quasi-first-order kinetic pathway [77]. Conversely, at lower dosages, the limited active sites may hinder the adsorption efficiency and photocatalytic reactions, leading to deviations from the ideal quasi-second-order behavior.

Therefore, it can be concluded that the photodegradation of TC in this study is better described using the quasi-first-order kinetic model, especially under optimized catalyst dosage conditions. This observation is consistent with the behavior typically reported for heterogeneous photocatalytic systems, where the reaction rate is typically controlled by the initial contaminant concentration and the availability of photocatalytic sites [78].

3.4 Utilizing photocatalysts again

The stability and recyclability of a photocatalyst are crucial to both its photocatalytic properties and potential applications. To evaluate photocatalyst stability, recycled photocatalysts were photodegraded under the same conditions. Before further use, the photocatalyst was collected after the photocatalytic reaction, washed with ethanol and distilled water, and dried in an oven set at 120 °C. As shown in Fig. 6, the recovered photocatalyst retained its high photocatalytic activity after five recycling cycles, with the tetracycline degradation efficiency decreasing to 70%. The decline in photocatalytic activity of the nanocatalyst was due to two reasons: either the pores of the composite photocatalyst were clogged or the photocatalyst was lost during the recycling process. The TC degradation efficiency on the carbon nanotube/Fe_2O_3/TiO_2/bentonite composites decreased from 95.1% to 70% after five recycling cycles. The main reason is the increased loss of CNT/Fe_2O_3/TiO_2/Bentonite photocatalysts during the process (because TC and intermediates were not completely decomposed during each previous cycle, some active sites were blocked or inactivated).

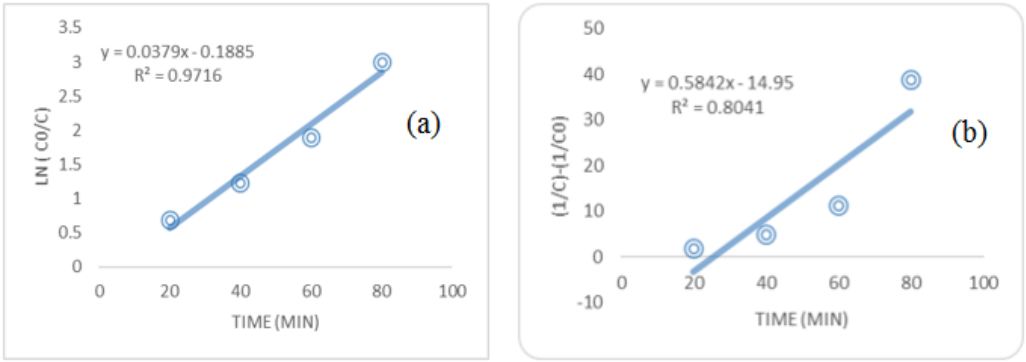

Figure 5. (a) Photodegradation of TC using a compound dosage = 15 mg/L, pH = 5, irradiation time = 120 min, and tetracycline hydrochloride (TC) concentration = 0.5 mg/L, with $R^2 = 0.9716$, according to a pseudo first-order kinetic analysis. (b) Using a compound nanodosage = 15 mg/L, pH = 5, irradiation time = 120 min, and tetracycline hydrochloride (TC) concentration = 0.5 mg/L, with $R^2 = 0.8041$, a pseudo second-order kinetic analysis is used for the photodegradation of TC.

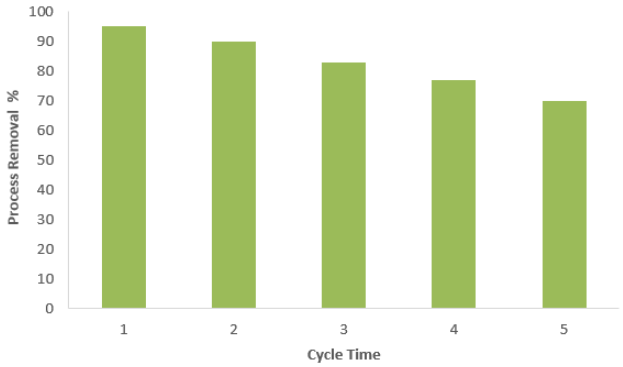

Figure 6. Effect of number of cycles on TC removal.

4. Conclusion

In batch processes, heterogeneous catalysts such as carbon nanotubes (CNTs)/iron oxide (Fe_2O_3)/titanium dioxide (TiO_2)/bentonite are used. Organic contaminants such as tetracycline hydrochloride (TC) were removed using a nanocomposite oxidizer and ultraviolet (UV) radiation. The tetracycline content was analyzed in a glass reactor under UV radiation. Titanium dioxide nanoparticles are reliable and stable semiconductors and highly effective oxidizing agents for the removal of organic contaminants. They are supported by non-metallic materials, such as multi-walled carbon nanotubes (MWCNTs), which have the ability to conduct electron recombination by stabilizing and trapping the electrons of TiO, resulting in electron pair separation. Iron oxide (FeO_3) acts as an additional catalyst to enhance electron transfer and cracking efficiency, while promoting the formation of oxidizing radicals ($^{\bullet}OH$). Bentonite enhances the catalyst surface dispersion and acts as a support. The optimum operating conditions for the batch treatment system were pH 5 and a catalyst weight of 15 mg/L of nanocomposite. As a result, the tetracycline hydrochloride content was removed with an efficiency of 95.1% at a concentration of 0.5 ppm. In the batch treatment system, the effects of irradiation time, TC concentration, nanocomposite dosage, pH, and process kinetics were studied.

Acknowledgment

This work was supported financially by the university of technology of the Ministry of Education of Iraq.

Authors contributions
Authors have contributed equally in preparing and writing the manuscript.

Availability of data and materials
The data that support the findings of this study are available from the corresponding author, upon reasonable request.

Conflict of interests
The author declare that they have no known competing financial interests or personal relationships that could have appeared to influence the work reported in this paper.

References

[1] Q. Zhou, Z. Ji, H. Yu, S. Lu, J. Guo, and C. Wu. *Langmuir*, **40**(2024): 7078–7086, .
DOI: https://doi.org/10.1021/acs.langmuir.4c00203.

[2] Y. Zhao, L. Chang, Y. Li, W. He, K. Liu, M. Cui, M. U. Hameed, and J. Xie. *J. Water Process Eng.*, **53**(2023):103753.
DOI: https://doi.org/10.1016/j.jwpe.2023.103753.

[3] M. J. A. Alatabe M. Ahmadlouydarab A. D. Jaafar, M. S. Graish and R. N. Aldain. *Desalination and Water Treatment*, **320**(2024): 100885.
DOI: https://doi.org/10.1016/j.dwt.2024.100885.

[4] R. Wang, M. Ji, H. Zhai, Y. Guo, and Y. Liu. *Sci. Total Environ.*, **796**(2021):148919, .
DOI: https://doi.org/10.1016/j.scitotenv.2021.148919.

[5] L.-T. Allan-Blitz and K. H. Mayer. *Current HIV/AIDS Reports*, **22**(2025):1–11.
DOI: https://doi.org/10.1007/s11904-024-00709-w.

[6] N. Bhatia, J. D. Rosso, L. S. Gold, E. Lain, Z. D. Draelos, and S. Sidgiddi. *JAMA dermatology*, **161**(2025):499–507.
DOI: https://doi.org/10.1001/jamadermatol.2024.6542.

[7] H. Tahmasebi, N. Arjmand, M. Momeni, A. Babaeizad, F. Alibabaei, N. Alibabaei, A. Bahar, V. Oksenych, and M. Eslami. *Biomolecules*, **15**(2025):93.
DOI: https://doi.org/10.3390/biom15010093.

[8] D.-D. Zhu, X. R. Li, T. F. Ma, J. Q. Chen, C. H. Ge, S. H. Yang, W. Zhang, J. Chen, J. J. Zhang, M. M. Qi, L. Zhang, and H. J. Yang. *Microb. Res.*, **16**(2025):59.
DOI: https://doi.org/10.3390/microbiolres16030059.

[9] Z. Liu, Q. Zhou, J. Xue, M. Cui, L. Xu, T. Fang, Z. Wen, D. Li, J. Wang, X. Deng, and Y. Zhou. *Biochem. Pharma*, **231**(2025): 116638, .
DOI: https://doi.org/10.1016/j.bcp.2024.116638.

[10] S. ul Malook, A. K. Arora, and A. C. N. Wong. *Current Opinion in Insect Science*, **69**(2025):101346.
DOI: https://doi.org/10.1016/j.cois.2025.101346.

[11] M. D. N. Maurya, M. M. Mishra, M. P. A. Chinchole, S. Jain, and S. Chinta. *TEXTBOOK OF MEDICINAL CHEMISTRY-III*, (2025).

[12] R. Sheikhsamany, A. Nezamzadeh-Ejhieh, R. Ensandoost, and B. Kakavandi. *J. Mol. Liq.*, **403**(2024):124850, .
DOI: https://doi.org/10.1016/j.molliq.2024.124850.

[13] K. E. Bentum, E. Kuufire, R. Nyarku, V. Osei, S. Price, D. Bourassa, T. Samuel, C. R. Jackson, and W. Abebe. *Zoonotic Diseases*, **5**(2025): 4.
DOI: https://doi.org/10.3390/zoonoticdis5010004.

[14] A. V. Alyokhin, B. M. Rosenthal, D. C. Weber, and M. B. Baker. *Biological Rev.*, **100**(2025):1067–1082.
DOI: https://doi.org/10.1111/brv.13174.

[15] M. Ahmad, K. Wu, A. Ahmed, M. Adnan, M. Rafiq, and B. Yu H. Cong. *J. Mater. Chem. A*, **13**(2025):6223–6273.
DOI: https://doi.org/10.1039/D4TA08155B.

[16] I. N. S. Kahar, S. A. Idrus-Saidi, N. Othman, M. A. A. M. Akta, M. A. A. Zaini, and A. Rosli. *Malaysian J. Fundament. Appll. Sci.*, **21**(2025):1874–1882.
DOI: https://doi.org/10.11113/mjfas.v21n2.3754.

[17] H. Derikvandi, M. Vosough, and A. Nezamzadeh-Ejhieh. *Inter. J. Hydrogen Ener.*, **46**(2021):2049–2064.
DOI: https://doi.org/10.1016/j.ijhydene.2020.10.065.

[18] S. Shao and X. Wu. *Critical reviews in biotechnology*, **40**(2020): 1010–1018.
DOI: https://doi.org/10.1080/07388551.2020.1805585.

[19] J. Cheng, Y. Xie, Y. Wei, D. Xie, W. Sun, Y. Zhang, M. Li, and J. An. *Chemosphere*, **286**(2022):131841.
DOI: https://doi.org/10.1016/j.chemosphere.2021.131841.

[20] R. M. Al-Maliki, B. M. Ibraheem, and S. Bassim. *Petroleum Chem.*, **64**(2024):972–980.
DOI: https://doi.org/10.1134/S0965544124070119.

[21] X. Yang, W. Wang, S. Feng, L. Jin, T. J. Lu, Y. Chai, and Q. Zhang. *Energy Procedia*, **88**(2016):566–573, .
DOI: https://doi.org/10.1016/j.egypro.2016.06.079.

[22] C. Lu, W. Guan, G. Zhang, L. Ye, Y. Zhou, and X. Zhang. *Micro Nano Lett.*, **8**(2013):749–752.
DOI: https://doi.org/10.1049/mnl.2013.0428.

[23] S. Salesi and A. Nezamzadeh-Ejhieh. *Environ. Sci. Pollut. Res.*, **30**(2023):105440–105456.
DOI: https://doi.org/10.1007/s11356-023-29730-z.

[24] Z. Zhang M. Zhang J. Mu Z. Guo Y. Liu P. Zhang, C. Shao. *Nanoscale*, **3**(2011):2943–2949.
DOI: https://doi.org/10.1039/C1NR10269A.

[25] C.-T. Wang, W.-L. Chou, M.-H. Chung, and Y.-M. Kuo. *Desalination*, **253**(2010):129–134, .
DOI: https://doi.org/10.1016/j.desal.2009.11.020.

[26] F. Azadi, A. Pourahmad, Sh. Sohrabnezhad, and M. Nikpassand. *D. Engi, Simulation*, **44**(1985):66–74.
DOI: https://doi.org/10.1177/003754978504400202.

[27] A. Jiménez-Vázquez, R. Jaimes-López, C. M. Morales-Bautista, S. Pérez-Rodríguez, Y. Gochi-Ponce, and L. A. Estudillo-Wong. *Catalysts*, **15**(2025):236.
DOI: https://doi.org/10.3390/catal15030236.

[28] T. Shahzad, S. Nawaz, H. Jamal, T. Shahzad, F. Akhtar, and U. Kamran. *J. Composit. Sci.*, **9**(2025):18.
DOI: https://doi.org/10.3390/jcs9010018.

[29] M. Yang, H. Li, C. Yang, H. Li, Y. Pang, and Y. Chen. *Bioresource Technology Reports*, **29**(2025):102076, .
DOI: https://doi.org/10.1016/j.biteb.2025.102076.

[30] S. Yadav, N. Sharma, A. Dalal, P. Panghal, A. K. Sharma, and S. Kumar. *Environ. Monitoring Assessment*, **197**(2025):1–37.
DOI: https://doi.org/10.1007/s10661-025-13657-8.

[31] V. Kanchana, S. Vasanthan, L. Mayavan, and A. Kistan. *J. Electronic Mater.*, **54**(2025):1–13.
DOI: https://doi.org/10.1007/s11664-025-11739-4.

[32] N. L. Sharon, S. Kannan, T. Abisheik, M. Tiffany, V. Pandiyan, G. Periyasami, P. Barmavatu, K. Shanmugaraj, and K. Balu. *J. Allo. Comp.*, **1020**(2025):179389.
DOI: https://doi.org/10.1016/j.jallcom.2025.179389.

[33] H. Hidayat, N. Mufti, K. L. Permatasari, A. S. P. Dewi, and P. Puspitasari. *AIP Conference Proceedings*, **3197**(2025):020015.
DOI: https://doi.org/10.1063/5.0241072.

[34] Z. Zhang, Y. Guo, F. Long, X. Zhang, J. Wang, and Y. Ren. *J. Environ. Chem. Eng.*, **13**(2025):115750, .
DOI: https://doi.org/10.1016/j.jece.2025.115750.

[35] R. Prasetyowati, R. I. SAaputri, E. F. M. Harahap, P. E. Swastika, F. Fauzi, W. S. B. Dwandaru, A. Ariswan, M. Riswan, and E. Widianto. *Emergent Mater.*, **2025**(2025):1–14.
DOI: https://doi.org/10.1007/s42247-025-01005-y.

[36] S. Yang, J. Gu, B. Dai, and L. Zhang. *ChemSusChem*, **18**(2025):e202401115, .
DOI: https://doi.org/10.1002/cssc.202401115.

[37] D. Li, C. Wang, J. Zhang, P. Zhan, Z. Liu, S. Liu, H. Deng, and X. Peng. *Colloids and Surfaces A: Physicochemical and Engineering Aspects*, **715**(2025):136407, .
DOI: https://doi.org/10.1016/j.colsurfa.2025.136407.

[38] F. Wang, Y. Gao, Y. Chai, C. C. Wang, J. F. Wang, X. H. Yi, Y. Li, H. Fu, C. Zhao, and P. Wang. *Appl. Catal. B: Environ. Energy*, **364**(2025):124848, .
DOI: https://doi.org/10.1016/j.apcatb.2024.124848.

[39] S. Xu, S. Zhang, H. Zhao, B. Liu, and Y. Zhang. *Catal. Lett.*, **155**(2025):1–14.
DOI: https://doi.org/10.1007/s10562-025-04939-4.

[40] C.-H. Hu, J. Hu, H.-Y. Liu, and F.-P. Jiao. *Indust. Eng. Chem. Res.*, **64**(2025):2636–2646.
DOI: https://doi.org/10.1021/acs.iecr.4c03622.

[41] J. Gautam, S. Lee, and S. Park. *Adv. Energ. Mater.*, **15**(2025):2406047.
DOI: https://doi.org/10.1002/aenm.202406047.

[42] S. A. Mirsalari, A. Nezamzadeh-Ejhieh, and A. R. Massah. *Environ. Sci. Pollut. Res.*, **29**(2022):1–20.
DOI: https://doi.org/10.1007/s11356-021-17569-1.

[43] H. Yao, J. Zeng, Y. Wang, and Z. You. *ACS Appl. Nano Mater.*, **8**(2025):5254–5274.
DOI: https://doi.org/10.1021/acsanm.4c06153.

[44] M. jaafar Al-atabi. *Inter. J. Integ. Eng.*, **10**(2018):96–102.
DOI: https://doi.org/10.30880/ijie.2018.10.01.015.

[45] A. A. A. Ayad Dari Jaafar and B. J. Kadhim. *J. Mech. Eng. Res. Develop.*, **44**(2021):66–74.

[46] B. Huo, S. Liu, C. Du, F. Kuang, Y. Lv, X. Wu, P. Liu, L. Liang, G. Chen, and C. Y. Guo. *Chem. Eng. J.*, **506**(2025):160213.
DOI: https://doi.org/10.1016/j.cej.2025.160213.

[47] J. Zhang, X. Wang, X. Wang, and C. Li. *Acc. Chem. Res.*, **58**(2025):787–798, .
DOI: https://doi.org/10.1021/acs.accounts.4c00582.

[48] P. Ningthoukhongjam, C. S. Gopinath, and R. G. Nair. *Inter. J. Hydrog. Ener.*, **113**(2025):133–146.
DOI: https://doi.org/10.1016/j.ijhydene.2025.02.395.

[49] X. Sun, H. Yang, J. Xie, G. Teng, J. He, Z. Zhao, and C. Zhang. *Water Res.*, **278**(2025):123345, .
DOI: https://doi.org/10.1016/j.watres.2025.123345.

[50] L. Sun, X. He, B. Liu, S. Zhang, Z. Xiang, X. Wang, and Y. Wang. *Separ. Purif. Tech.*, **353**(2025):128515, .
DOI: https://doi.org/10.1016/j.seppur.2024.128515.

[51] X. Li, Y. Liu, M. Yao, and F. Liu. *Mol. Catal.*, **573**(2025):114815, .
DOI: https://doi.org/10.1016/j.mcat.2025.114815.

[52] Z. Liu, M. Zhu, Z. Wang, H. Wang, C. Deng, and K. Li. *Materials*, **9**(2016):364, .
DOI: https://doi.org/10.3390/ma9050364.

[53] Z. A. Suliman, A. C. Mecha, and J. I. Mwasiagi. *Discover Chemistry*, **2**(2025):32.
DOI: https://doi.org/10.1007/s44371-025-00104-3.

[54] M. Ahmadi, H. R. Motlagh, N. Jaafarzadeh, A. Mostoufi, R. Saeedi, G. Barzegar, and S. Jorfi. *J. Environ. Manag.*, **186**(2017):55–63.
DOI: https://doi.org/10.1016/j.jenvman.2016.09.088.

[55] X. Cao, S. Luo, C. Liu, and J. Chen. *Adv. Powder Tech.*, **28**(2017):993–999.
DOI: https://doi.org/10.1016/j.apt.2017.01.003.

[56] G. H. Safari, M. Hoseini, M. Seyedsalehi, J. Jaafari H. Kamani, and A. H. Mahvi. *Inter. J. Environ. Sci. Tech.*, **12**(2015):603–616.
DOI: https://doi.org/10.1007/s13762-014-0706-9.

[57] S. Raheem, A. Aziz, A.-R. Ayad, D. Jaafar, and A. Lect. *J. Eng.*, **23**(2017).
DOI: https://doi.org/10.31026/j.eng.2017.03.03.

[58] M. N. Shaddad, A. A. Alanazi, A. M. Aldawsari, M. A. Alotaibi, S. A. Aladeemy, F. Abdulaziz, and Y. S. Aljohani. *J. Indust. Eng. Chem.*, (2025).
DOI: https://doi.org/10.1016/j.jiec.2025.04.050.

[59] S. Kaushal, N. Thakur, and K. Kumar. *Inter. J. Environ. Anal. Chem.*, **2025**(2025):1–23.
DOI: https://doi.org/10.1080/03067319.2025.2494062.

[60] P. L. Tran-Nguyen, K. P. Ly, S. P. Santoso, N. P. D. Tran, A. E. Angkawijaya, H. N. Nguyen, Q. K. Huynh, and N. T. N. Mai. *J. Chem. Tech. Biotech.*, **100**(2025):1222–1237.
DOI: https://doi.org/10.1002/jctb.7857.

[61] D. Anwar, N. al kaisy, and B. Azhdar. *Mater. Res. Express.*, **12**(2025): 045402.
DOI: https://doi.org/10.1088/2053-1591/adcdce.

[62] F. Alizadeh, M. Ghorbanpour, and M. J. A. Alatabe. *Indian Chem. Eng.*, **66**(2024):1–12.
DOI: https://doi.org/10.1080/00194506.2024.2335332.

[63] F. A. Abbasi, S. M. A. Shah, M. Mustafa, U. Humayun, M. Ayubi, Z. A. Arfeen, S. M. Lalji, S. L. Ali, and M. Mateen. *Multiscale Multidisciplinary Modeling, Experiments Design*, **8**(2025).
DOI: https://doi.org/10.1007/s41939-025-00770-x.

[64] N. Swadchaipong, V. Tongnan, A. Makdee, U. W. Hartley, and I. Sereewatthanawut. *Catalysts*, **15**(2025):153.
DOI: https://doi.org/10.3390/catal15020153.

[65] R. Sheikhsamany, A. Nezamzadeh-Ejhieh, and R. S. Varma. *Surf. Interf.*, **54**(2024):105205, .
DOI: https://doi.org/10.1016/j.surfin.2024.105205.

[66] L.-B. Zhu and S.-N. Ding. *Anal. Chem.*, **97**(2025):7546–7554.
DOI: https://doi.org/10.1021/acs.analchem.5c01132.

[67] M. Hajji, A. Akkari, A. Garcia-Loureiro, and N. T. Kamoun. *Chemistry Africa*, **2025**(2025):1–14.
DOI: https://doi.org/10.1007/s42250-025-01252-w.

[68] M. J. A. Alatabe, M. A. R. Hameed, and K. M. M. Al-zobai. *Int. J. Appl. Sci. Eng.*, **18**(2021):1–11.
DOI: https://doi.org/10.6703/IJASE.202109_18(5).003.

[69] M. Tang, Y. Xia, D. Yang, J. Liu, X. Zhu, and R. Tang. *Mater.*, **14**(2021):5674.
DOI: https://doi.org/10.3390/ma14195674.

[70] K. Kumari, S. R. Mishra, V. Gadore, N. S. Moyon, and M. Ahmaruzzaman. *J. Inorg. Organometal. Polymers Mater.*, (2025):1–24.
DOI: https://doi.org/10.1007/s10904-025-03700-z.

[71] T. Luo, H. Feng, L. Tang, Y. Lu, W. Tang, S. Chen nad J. Yu, Q. xie, and X. Ouyang Z. Chen. *Chem. Eng. J.*, **382**(2020):122970.
DOI: https://doi.org/10.1016/j.cej.2019.122970.

[72] M. Pelaez, N. T. Nolan, S. C. Pillai, M. K. Seery, P. Falaras, A. G. Kontos, P. S. M. Dounlop, J. W. J. Hamilton, J. A. Byrne, K. O'Shea, M. H. Entezari, and D. D. Dionysio. *Appl. Catal. B: Environ.*, **125**(2012):331–349.
DOI: https://doi.org/10.1016/j.apcatb.2012.05.036.

[73] M. M. Rahman, S. B. Khan, A. Jamal, M. Faisal, and A. M. Aisiri. "iron oxide nanoparticles,". *Nanomaterials*, **3**(2011):43–67.
DOI: https://doi.org/10.5772/27698.

[74] J. Amaya, L. Bobadilla, L. Azancot, M. Centeno, S. Moreno, and R. Molina. *Mater. Res. Bullet.*, **123**(2020):110728.
DOI: https://doi.org/10.1016/j.materresbull.2019.110728.

[75] T. Wang, L. Xue, Y. Liu, T. Fang, L. Zhang, and B. Xing. *Chem. Eng. J.*, **435**(2022):134822, .
DOI: https://doi.org/10.1016/j.cej.2022.134822.

[76] N. Omrani, A. Nezamzadeh-Ejhieh, and M. Alizadeh. *Desalination Water Treatment*, **162**(2019):290–302.
DOI: https://doi.org/10.5004/dwt.2019.24352.

[77] C. Zhou, L. Tao, J. Gao, J. Dong, Q. Zhu, C. Liao, and G. Jiang. *J. Environ. Chem. Eng.*, **12**(2024):113370, .
DOI: https://doi.org/10.1016/j.jece.2024.113370.

[78] S. Sharafzadeh, J. Zolgharnein, A. Nezamzadeh–Ejhieh, and S. D. Farahani. *Inter. J. Hydrogen Energ.*, **106**(2025):1429–1442.
DOI: https://doi.org/10.1016/j.ijhydene.2025.02.031.